RESEARCH ARTICLE SUMMARY

CARBON CYCLE

Contrasting carbon cycle responses of the tropical continents to the 2015–2016 El Niño

Junjie Liu,* Kevin W. Bowman, David S. Schimel, Nicolas C. Parazoo, Zhe Jiang, Meemong Lee, A. Anthony Bloom, Debra Wunch, Christian Frankenberg, Ying Sun, Christopher W. O'Dell, Kevin R. Gurney, Dimitris Menemenlis, Michelle Gierach, David Crisp, Annmarie Eldering

INTRODUCTION: The influence of El Niño on climate is accompanied by large changes to the carbon cycle, and El Niño–induced variability in the carbon cycle has been attributed mainly to the tropical continents. However, owing to a dearth of observations in the tropics, tropical carbon fluxes are poorly quantified, and considerable debate exists over the dominant mechanisms (e.g., plant growth, respiration, fire) and regions (e.g., humid versus semiarid tropics) on the net carbon balance.

RATIONALE: The launch of the Orbiting Carbon Observatory-2 (OCO-2) shortly before the 2015–2016 El Niño, the second strongest since the 1950s, has provided an opportunity to understand how tropical land carbon fluxes respond to the warm and dry climate characteristics of El Niño conditions. The El Niño events may also provide a natural experiment to study the response of tropical land carbon fluxes to future climate changes, because anomalously warm and dry tropical environments typical of El Niño are expected to be more frequent under most emission scenarios.

RESULTS: The tropical regions of three continents (South America, Asia, and Africa) had heterogeneous responses to the 2015–2016 El Niño, in terms of both climate drivers and the carbon cycle. The annual mean precipitation over tropical South America and tropical Asia was lower by 3.0σ and 2.8σ, respectively, in 2015 relative to the 2011 La Niña year. Tropical Africa, on the other hand, had near equal precipitation and the same number of dry months between 2015 and 2011; however, surface temperatures were higher by 1.6σ, dominated by the positive anomaly over its eastern and southern regions. In response to the warmer and drier climate anomaly in 2015, the pantropical biosphere released 2.5 ± 0.34 gigatons more carbon into the atmosphere than in 2011, which accounts for 83.3% of the global total 3.0–gigatons of carbon (gigatons C) net biosphere flux differences and 92.6% of the atmospheric CO_2 growth-rate differences between 2015 and 2011. It indicates that the tropical land biosphere flux anomaly was the driver of the highest atmospheric CO_2 growth rate in 2015. The three tropical continents had an approximately even contribution to the pantropical net carbon flux anomaly in 2015, but had diverse dominant processes: gross primary production (GPP) reduced carbon uptake (0.9 ± 0.96 gigatons C) in tropical South America, fire increased carbon release (0.4 ± 0.08 gigatons C) in tropical Asia, and respiration increased carbon release (0.6 ± 1.01 gigatons C) in Africa. We found that most of the excess carbon release in 2015 was associated with either extremely low precipitation or high temperatures, or both.

CONCLUSION: Our results indicate that the global El Niño effect is a superposition of regionally specific effects. The heterogeneous climate forcing and carbon response over the three tropical continents to the 2015–2016 El Niño challenges previous studies that suggested that a single dominant process determines carbon cycle interannual variability, which could also be due to previous disturbance and soil and vegetation structure. The similarity between the 2015 tropical climate anomaly and the projected climate changes imply that the role of the tropical land as a buffer for fossil fuel emissions may be reduced in the future. The heterogeneous response may reflect differences in temperature and rainfall anomalies, but intrinsic differences in vegetation species, soils, and prior disturbance may contribute as well. A synergistic use of multiple satellite observations and a long time series of spatially resolved fluxes derived from sustained satellite observations will enable tests of these hypotheses, allow for a more process-based understanding, and, ultimately, aid improved carbon-climate model projections. ■

ON OUR WEBSITE

Read the full article at http://dx.doi.org/10.1126/science.aam5690

The list of author affiliations is available in the full article online.
*Corresponding author. Email: junjie.liu@jpl.nasa.gov
Cite this article as J. Liu *et al.*, *Science* **358**, eaam5690 (2017). DOI: 10.1126/science.aam5690

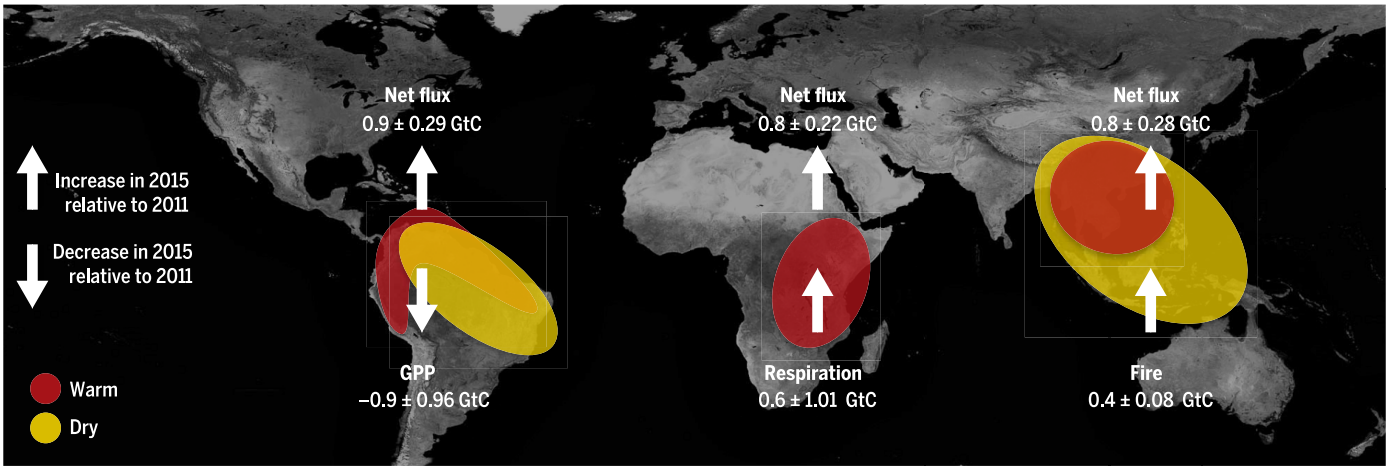

Diverse climate driver anomalies and carbon cycle responses to the 2015–2016 El Niño over the three tropical continents. Schematic of climate anomaly patterns over the three tropical continents and the anomalies of the net carbon flux and its dominant constituent flux (i.e., GPP, respiration, and fire) relative to the 2011 La Niña during the 2015–2016 El Niño. GtC, gigatons C.

RESEARCH ARTICLE

CARBON CYCLE

Contrasting carbon cycle responses of the tropical continents to the 2015–2016 El Niño

Junjie Liu,[1]* Kevin W. Bowman,[1] David S. Schimel,[1] Nicolas C. Parazoo,[1] Zhe Jiang,[2] Meemong Lee,[1] A. Anthony Bloom,[1] Debra Wunch,[3] Christian Frankenberg,[1,4] Ying Sun,[1]† Christopher W. O'Dell,[5] Kevin R. Gurney,[6] Dimitris Menemenlis,[1] Michelle Gierach,[1] David Crisp,[1] Annmarie Eldering[1]

The 2015–2016 El Niño led to historically high temperatures and low precipitation over the tropics, while the growth rate of atmospheric carbon dioxide (CO_2) was the largest on record. Here we quantify the response of tropical net biosphere exchange, gross primary production, biomass burning, and respiration to these climate anomalies by assimilating column CO_2, solar-induced chlorophyll fluorescence, and carbon monoxide observations from multiple satellites. Relative to the 2011 La Niña, the pantropical biosphere released 2.5 ± 0.34 gigatons more carbon into the atmosphere in 2015, consisting of approximately even contributions from three tropical continents but dominated by diverse carbon exchange processes. The heterogeneity of the carbon-exchange processes indicated here challenges previous studies that suggested that a single dominant process determines carbon cycle interannual variability.

The influence of an El Niño on climate is accompanied by large changes to the carbon cycle. The growth rate of atmospheric CO_2 increases during El Niño years, indicating reduced net CO_2 uptake from the atmosphere (*1*–*3*). The persistent response of the carbon cycle to the El Niño provides direct evidence of the carbon-climate feedbacks (*4*). El Niño–induced variability in the carbon cycle has been attributed mainly to the interannual variability of land-atmosphere CO_2 fluxes, most likely in the tropics (*1*–*3*). Likewise, climate models simulate the response of tropical rainforests to warming and drying as dominant carbon-climate feedbacks (*4*–*6*). Owing to a dearth of observations over the tropics (*7*, *8*), however, tropical carbon fluxes are poorly quantified, and considerable debate exists over the dominant mechanisms (e.g., plant growth, respiration, fire) and regions (e.g., humid versus semiarid tropics) on the net balance (*2*, *9*–*11*). The launch of the Orbiting Carbon Observatory-2 (OCO-2) (*12*) shortly before the 2015–2016 El Niño, the second strongest since the 1950s (www.esrl.noaa.gov/psd/data/correlation/nina34.data), provides an opportunity to understand how tropical land carbon fluxes respond to the warm and dry climate characteristics of the El Niño conditions. The El Niño events may also provide a natural experiment to study the response of tropical land carbon fluxes to future climate change, because anomalously warm and dry tropical environments typical of El Niño conditions are expected to be more frequent under most emission scenarios (*13*–*15*).

The 2015–2016 El Niño started at the end of 2014, peaked in late 2015, and ended in May 2016 (fig. S1). It lasted 19 months, which is 6 months longer than the 1997–1998 El Niño, the strongest El Niño on record. Although tropical land is generally warmer and drier during an El Niño, the climate anomaly over the three tropical continents (i.e., tropical South America, Africa, and Asia) was quite heterogeneous (*16*). In response to the 2015–2016 El Niño event, the gross primary production (GPP)–weighted annual mean precipitation anomalies in 2015 were 2.1σ and 1.7σ below the 30-year climatological mean for tropical South America and Asia, respectively (fig. S2). Whereas the tropical African precipitation anomaly was within climate variability, the GPP-weighted annual mean surface-skin temperature had an anomaly of 1.0σ (fig. S2). These anomalies have likely caused the historically high atmospheric CO_2 growth rate in 2015 (*17*).

Here, to study the impact of the 2015–2016 El Niño on the carbon cycle, we contrasted the carbon flux response to that of the 2011 La Niña, with a rationale that the flux difference between El Niño and La Niña indicates a range of carbon cycle responses to an El Niño–Southern Oscillation (ENSO) cycle. The influence of climate on the carbon cycle is reflected in the airborne fraction (AF), which is the percentage of anthropogenic emissions that remain in the atmosphere (*18*). The average AF has been ~0.44 for decades (*19*), albeit with slight trends, but varies dramatically with the ENSO cycle (table S1), reflecting the effects of climate on terrestrial and marine carbon processes (*20*). During the 2011 La Niña, only 34% of anthropogenic emissions remained in the atmosphere (AF = 0.34), reflecting the strong land uptake outside the tropics (*21*), whereas in the El Niño year of 2015, 56% of emissions contributed to the atmospheric increase (AF = 0.56) (*19*). In this study, we quantified the anomaly of net biosphere exchange (NBE) and its constituent carbon fluxes, including GPP, biomass burning, and respiration, by assimilating multiple satellite observations independently into modeling frameworks. We also analyzed the relationship between climate driver (i.e., temperature and precipitation) anomalies and the carbon flux responses over the three tropical continents. We primarily focused on the responses in 2015, but briefly reviewed the NBE response during the peak 2015–2016 El Niño (May 2015 to April 2016). We found that the increase of NBE over the tropics was the main driver for the large atmospheric CO_2 growth rate and high AF in 2015 and that the three tropical continents showed diverse climate-driver anomalies and the corresponding carbon flux responses. During the peak of the 2015–2016 El Niño, tropical South America had the largest negative precipitation anomaly among the three tropical continents and the largest increase of net CO_2 release into the atmosphere relative to year 2011.

Climate-driver anomalies over tropical land in 2015 relative to 2011

Compared to 2011, tropical Asia and most of tropical South America experienced a negative precipitation anomaly that exceeded $\sqrt{2\sigma^2}$ (Fig. 1), and the dry season (monthly precipitation less than 100 mm) was lengthened by 1 to 3 months in 2015 (Fig. 1C). In contrast with the 2005 and 2010 Amazonia droughts, which mainly occurred over western and southern Amazonia and were linked to the increased tropical North Atlantic and central Pacific sea-surface temperature (*22*, *23*), the 2015 tropical South America drought was more severe in the northern and southeastern regions. Relative to 2011, the 2015 annual mean precipitation over tropical South America and tropical Asia was lower by 3.0σ and 2.8σ, respectively (Fig. 2). Tropical Africa, on the other hand, had near equal amounts of precipitation and the same number of dry months between 2015 and 2011 (Fig. 1), but with surface temperatures higher by 1.6σ (Fig. 2), dominated by the positive anomaly over the eastern and southern regions.

A framework to quantify NBE and its constituent fluxes

We quantified the regional carbon cycle responses to these heterogeneous climate anomalies

[1]Jet Propulsion Laboratory, California Institute of Technology, Pasadena, CA, USA. [2]National Center for Atmospheric Research, Boulder, CO, USA. [3]University of Toronto, Toronto, Ontario, Canada. [4]California Institute of Technology, Pasadena, CA, USA. [5]Colorado State University, Fort Collins, CO, USA. [6]Arizona State University, Tempe, AZ, USA.
†Present address: School of Integrative Plant Science, Soil and Crop Sciences Section, Cornell University, Ithaca, NY, USA.
*Corresponding author. Email: junjie.liu@jpl.nasa.gov

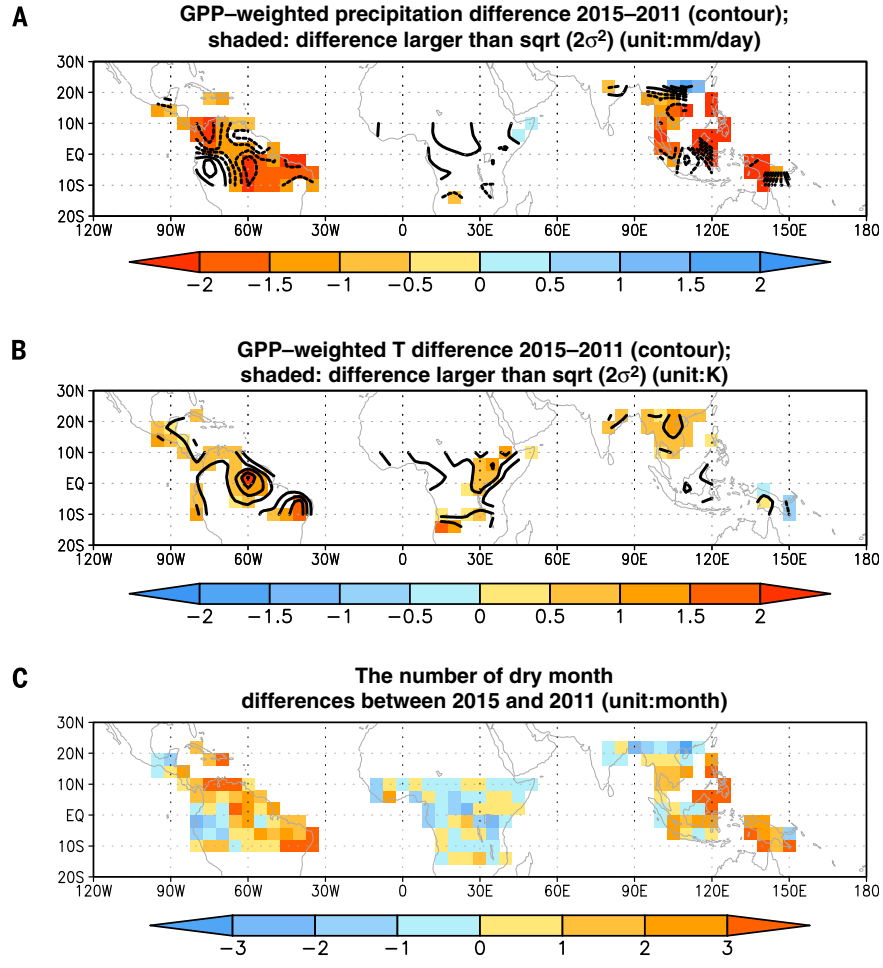

Fig. 1. Climate-driver anomaly. (**A**) The GPP-weighted annual mean precipitation (mm/day) between 2015 and 2011. (**B**) The GPP-weighted temperature (K) difference between 2015 and 2011. (**C**) The number of dry month differences between 2015 and 2011.

with a framework (fig. S6) that assimilated multiple satellite observations to constrain NBE and its constituent carbon fluxes, including GPP and biomass burning. The respiration was then calculated as a residual term, because NBE can be written as

$$\text{NBE} = \text{respiration} + \text{fire} - \text{GPP}$$

In the above equation, positive indicates that carbon is being released into the atmosphere. To constrain 2015–2016 and 2011 NBE, we assimilated column-averaged CO_2 dry-air mole fraction (X_{CO_2}) observations from the OCO-2 and Greenhouse Gases Observing Satellite (GOSAT) (*24*) separately into the NASA Carbon Monitoring System Flux (CMS-Flux) inversion system (*25*–*28*). Satellite X_{CO_2} observations are known to be affected by biases due to interfering atmospheric species. After bias correction, some effects may remain (*29*), so we performed a series of checks to ensure that the results were not artifacts of sampling and systematic differences between OCO-2 X_{CO_2} and GOSAT X_{CO_2}. Our checks included evaluation against X_{CO_2} from the Total Carbon Column Observing Network (TCCON) (*30*) (fig. S9) and CO_2 observations from aircraft and surface flasks [(*28*), figs. S11 to S13]. We showed [(*28*), supplementary text] that the relative differences between OCO-2 X_{CO_2} and GOSAT X_{CO_2} were negligible when both were compared to X_{CO_2} from TCCON (fig. S9). Using Observing System Simulation Experiments (OSSEs), which assimilated pseudo-observations that have the same samplings and errors as real observations, we showed [(*28*), supplementary text] that the posterior NBE differences resulting from the impact of sampling and the observation-error differences between the assimilated OCO-2 X_{CO_2} and GOSAT X_{CO_2} were within uncertainty (fig. S10). Because we used the same prior biosphere fluxes and uncertainties for 2011 and 2015–2016 (*28*), the posterior biosphere-flux differences were not sensitive to the prior biosphere fluxes. We showed (*28*) that the posterior NBE differences were only due to the differences in observations, the sensitivity of the observations to surface fluxes, and the observation error statistics.

To estimate GPP, we used a Bayesian analysis framework that optimally accounts for uncertainties in predictions of GPP from terrestrial biosphere models, satellite observations of solar-induced chlorophyll fluorescence (SIF) from GOSAT, and relationships between SIF and GPP (*31*, *32*, *28*). This GPP estimation approach has been used to examine large-scale GPP distributions and regional GPP responses to climate variability and drought, and has been extensively validated against flux tower data (*32*, *33*).

The biomass burning fluxes were optimized with CO observations from Measurements of Pollution in the Troposphere (MOPITT) (*34*, *35*). The carbon fluxes from biomass burning are then estimated as a multiplication between CO_2: CO emission ratio and the CO carbon fluxes. The emission ratio for peat fire over Indonesia is based on field measurements from (*36*). The NBE, GPP, and biomass burning fluxes were optimized independently. The more detailed methods are described in (*28*).

Response of NBE and its constituent fluxes over three tropical continents

We found that the higher AF in 2015 was primarily due to less land carbon uptake (i.e., more land carbon release) over the tropics. In total, the tropics released 2.5 ± 0.34 gigatons more carbon into the atmosphere in 2015 than in 2011 (Fig. 2). The tropics NBE anomaly in 2015 accounts for 83.3% of the global total 3.0 gigatons of carbon (gigatons C) NBE difference; it is equivalent to the atmospheric CO_2 growth rate difference between 2015 and 2011 (table S1). This effect was spread over the three tropical continents with 0.9 ± 0.29, 0.8 ± 0.22, and 0.8 ± 0.28 gigatons C over tropical South America, Africa, and Asia, respectively. During the peak 2015–2016 El Niño between May 2015 and April 2016, the tropics released 3.3 ± 0.34 gigatons more carbon into the atmosphere than in 2011 (Fig. 3), which was even more than was released in 2015. Tropical South America had the largest NBE anomaly (Fig. 3), with 1.6 ± 0.29 gigatons more carbon released into the atmosphere than in 2011, which corresponded to a 3.7σ negative precipitation anomaly and a 2.3σ positive temperature anomaly.

Even though the three tropical continents had comparable NBE anomalies in 2015 relative to 2011, different processes dominated in each region. Increased carbon release in tropical Asia was dominated by biomass burning emissions as constrained by MOPITT CO observations (*28*). The fire increase (0.4 ± 0.08 gigatons C) accounted for about half of the NBE increase (Fig. 2). We estimated that the biomass burning flux over tropical Asia was 0.5 ± 0.04 gigatons C in 2015, consistent with independent estimates ranging from 0.34 to 0.90 gigatons C over Indonesia (*37*, *38*). Unlike the 1997–1998 El Niño, when Indonesian fires dominated the pantropical land flux anomaly (*39*), in 2015, Indonesian fires contributed only 16% to the total tropical NBE anomaly. Negative GPP anomalies in tropical Asia (0.3 ± 0.76 gigatons C) corresponding to reduced precipitation and higher temperatures are not statistically significant; this is a consequence of the sparse GOSAT SIF observations over the region (fig. S9).

In tropical South America, the GPP reduction was the dominant driver for the NBE change

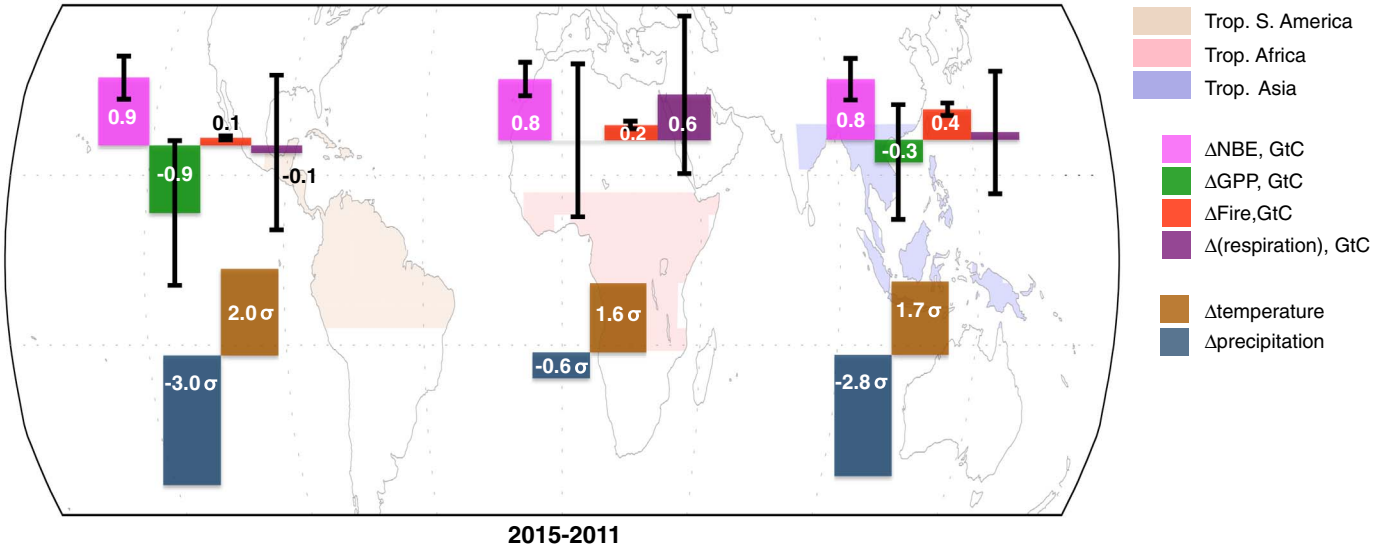

Fig. 2. Carbon flux, temperature, and precipitation anomalies in 2015 relative to 2011. Magenta, red, and purple bars are NBE, biomass burning (fire), and respiration differences between 2015 and 2011. Upward (positive) bars represent increased carbon release into the atmosphere in 2015 relative to 2011. The green bars show the GPP differences between 2015 and 2011. Downward (negative) bars represent less carbon uptake through photosynthesis in 2015 relative to 2011. The error bars are $\sqrt{\sigma^2_{2011}+\sigma^2_{2015}}$, where σ^2_{2011} and σ^2_{2015} are the error variances calculated from the optimization process (*28*). The dark blue bars represent precipitation differences, and the downward (negative) direction represents less precipitation in 2015 relative to 2011. The brown bars show temperature differences, with the upward (positive) direction representing higher temperatures in 2015 relative to 2011, where σ is 30-year (1981–2010) standard deviation. GtC, gigatons C.

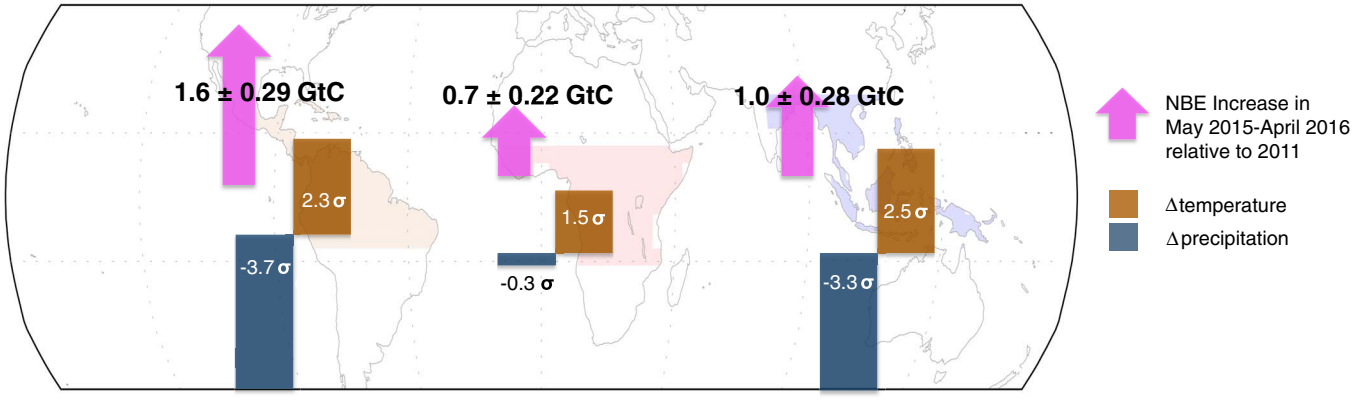

Fig. 3. NBE anomalies during the peak of the 2015–2016 El Niño (from May 2015 to April 2016) relative to 2011. NBE anomalies indicated by magenta arrows. Upward (positive) bars represent increased carbon release into the atmosphere during the peak of the 2015–2016 El Niño relative to 2011. The dark blue bars represent precipitation differences, and the downward (negative) direction represents less precipitation during the peak of the 2015–2016 El Niño relative to 2011. The brown bars show temperature differences, with the upward (positive) direction representing higher temperatures during the peak of the 2015–2016 El Niño relative to 2011, where σ is 30-year (1981–2010) standard deviation.

(Fig. 2): GPP was reduced by 0.9 ± 0.96 gigatons C and NBE increased by 0.9 ± 0.24 gigatons C, mainly owing to the lower than average precipitation (3.8σ) over the northern and southeastern part of the region (Fig. 4A) (*40*). Over these regions with extreme precipitation anomalies (i.e., larger than $\sqrt{2\sigma^2}$), the NBE increased by 1.0 ± 0.22 gigatons C and the GPP decreased by 0.7 ± 0.53 gigatons C (Fig. 4a). This implies that the rest of tropical South America, where the precipitation was slightly higher in 2015, absorbed 0.1 ± 0.13 gigatons more carbon from the atmosphere in 2015 than in 2011. This spatial gradient in carbon flux response suggests that the tropical South American carbon flux anomaly responded directly to precipitation anomalies. Leaf- and plot-level measurements also suggest that severe drought in the Amazon suppresses photosynthesis more than it suppresses respiration (*41*, *42*). The net carbon loss from the 2015–2016 drought over tropical South America was even higher than the 2010 Amazonia drought, which was estimated to range from 0.2 to 0.7 gigatons C relative to 2011 (*27*, *43*–*45*), whereas the carbon loss from the 2005 drought was estimated to be lower than from the 2010 drought (*46*).

High surface-temperature anomalies occurred in tropical Africa in 2015 (fig. S2), increasing the ecosystem respiration by 0.6 ± 1.01 gigatons C, which dominated the NBE response (75% of the 0.8 ± 0.22–gigatons C NBE difference). The large uncertainty in GPP led to the large uncertainty in the residual respiration. About 40% of the NBE

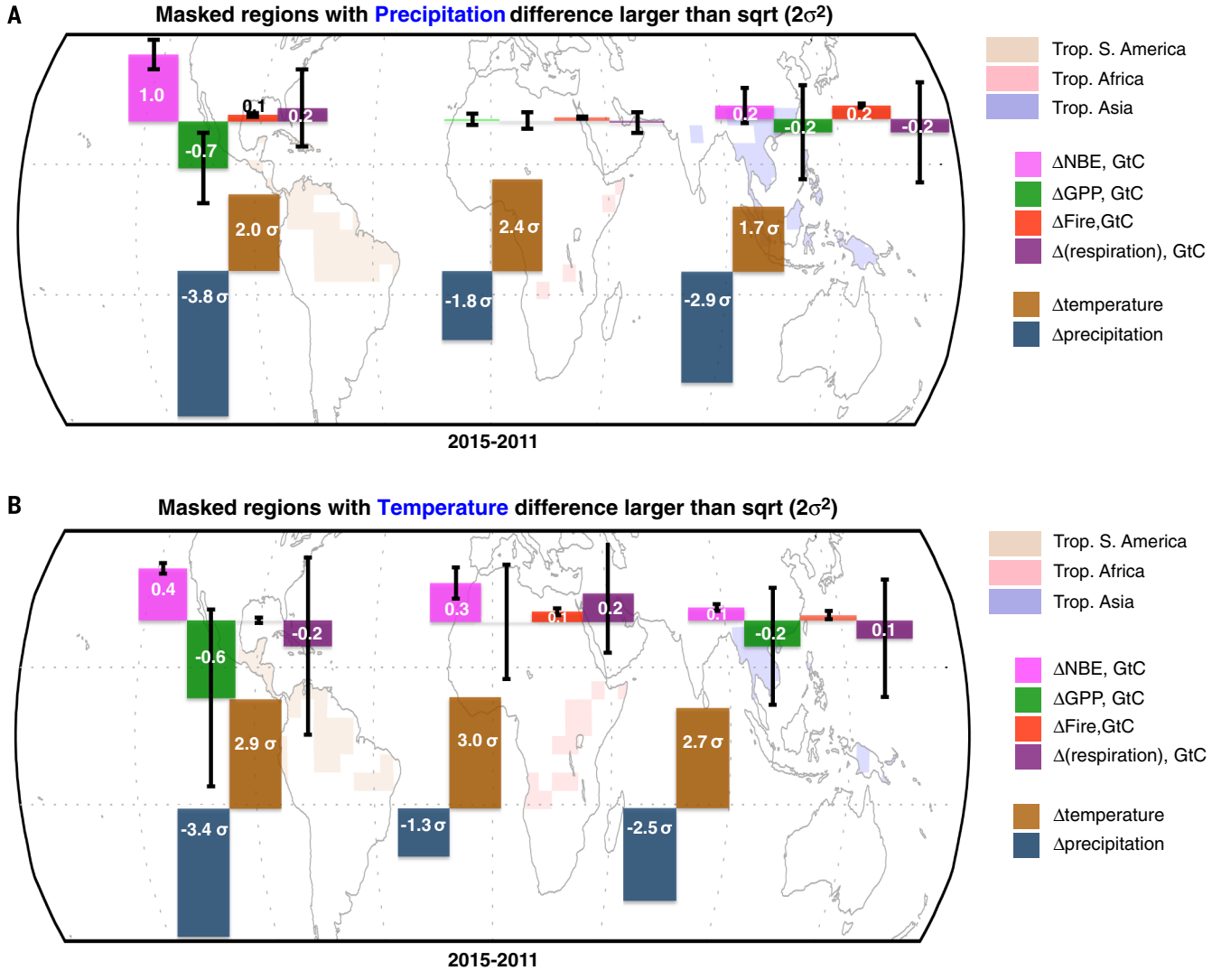

Fig. 4. The impact of extreme precipitation and temperature anomalies on carbon fluxes. Carbon flux differences between 2015 and 2011 over the three tropical land regions where either precipitation (**A**) or temperature (**B**) differences between 2015 and 2011 are larger than $\sqrt{2\sigma^2}$. The description of the color scheme is the same as for Fig. 2.

increase (0.3 ± 0.18 gigatons C) occurred in regions where temperature differences exceeded 3σ (Fig. 4B). Over central tropical Africa, which had historically nominal temperatures (Fig. 1B), the NBE change was close to neutral. The increase in ecosystem respiration accompanied by high surface temperatures is consistent with modeling studies that show that the variation in respiration over Africa was more closely related to temperature than to precipitation (*47*). A lack of ground-based observations over Africa makes it challenging to verify such a relationship.

Implications and outlook of future satellite CO_2 observing networks

Results from our study support the assumption in a number of studies (*2*, *3*, *48*) that the interannual variability of the global carbon cycle is dominated by the terrestrial tropics. However, our results indicate that the global El Niño effect is a superposition of regionally specific effects and reveal a more complex, mechanistic picture of the climate-carbon forcing response relationship than has been discussed to date [e.g., (*2*, *3*, *11*, *48*)]. Cox *et al.* (*2*) related the climate-land carbon feedback with ENSO-driven variability and proposed an emergent constraint on global carbon-climate feedback. The heterogeneous climate forcing and carbon response over the three tropical continents to the El Niño indicate the possibility of regionally dependent emergent constraints on carbon-climate feedback factors.

The larger precipitation anomaly in tropical South America and Asia, as compared to that in Africa, during the 2015–2016 El Niño was a typical response pattern to eastern Pacific El Niños. Malhi and Wright (*16*) analyzed the spatial variability of tropical land temperature and precipitation response to the El Niño over a 38-year period (1960–1998) and also found a stronger precipitation anomaly over tropical South America and Asia. Furthermore, the precipitation anomaly pattern over tropical South America in 2015 bears a remarkable similarity with the projected precipitation change at the end of century: decreased precipitation over the northern and southeastern region (*15*, *49*, *50*). Like in 2015, the eastern and southern regions of tropical Africa were projected to have more frequent heat waves in the future (*51*). The similarity between the 2015 tropical climate anomaly and the projected climate changes in the future imply an analog between the 2015 and the future tropical carbon cycle responses. Our study indicates that the impact of climate-driver changes on the carbon cycle may counteract the CO_2 fertilization effect over these regions (*10*, *18*), and the role of tropical land as a buffer for fossil fuel emissions may be reduced in the future. Indeed, some studies have shown that tropical land has acted as an increasing CO_2 source in recent decades with the increase of temperature and drought events (*52*, *53*). The

large fire emissions, mainly from peat land over tropical Asia in 2015, resulted from a combination of drought and land-use changes (*39*). Thus, the future fate of carbon in those peat lands, which store about 70 gigatons of organic carbon, could change with both climate change and policies of fire management and land use (*54*).

Most excess carbon released into the atmosphere in 2015 relative to 2011 was associated with either extremely low precipitation or high temperatures, or both (Fig. 4). Increasing evidence shows that drought events over tropical South America (*49*) and extreme heat events over parts of tropical Africa will most likely increase in the future (*51*). The role of extreme climate drivers in affecting the tropical carbon fluxes in 2015 further reinforces the importance of understanding the impact of these extreme events on the carbon cycle. In addition, an improved representation of extreme climate drivers in dynamical global vegetation models, which so far have been unable to represent short-term carbon losses from severe drought events, (*55*–*57*), is crucial to improving future climate projection (*58*–*60*).

The heterogeneity of the processes suggested by our study, in which respiration, GPP, and fire all play a role, challenges studies that suggest a single dominant process (*11*). The variability we observe within the 2015–2016 El Niño carbon cycle responses suggests that other El Niño events, where the resulting patterns of temperature and rainfall also varied (*16*), could result in different carbon cycle responses.

Aside from the difference in climate drivers, several other intrinsic differences between the continents may also contribute to the regionally dependent carbon cycle response to the 2015–2016 El Niño. We hypothesize that the differences in prior disturbance—resulting from different histories of drought and land use in the three regions, soil depth and texture, forest structure, and evolutionary differences in plant function between the continents (*16*, *61*)—may all have acted on the heterogeneous climate-driver anomalies, leading to the regionally dependent carbon cycle response. For instance, the elevation of tropical Africa is higher than the other two continents, and unlike Amazonia, the soil-fertility gradient in tropical Africa does not coincide with other gradients such as temperature (*62*). A longer period of data analysis is needed to test these different hypotheses.

Though OCO-2 and GOSAT provide unprecedented X_{CO_2} and SIF observations over the tropics, the 16-day (OCO-2) and 3-day (GOSAT) repeat cycles limit the spatiotemporal resolution of the inferred fluxes. The future OCO-3 and Geostationary Carbon Cycle Observatory (*63*) missions will further enhance observation coverage over the tropics. In addition to X_{CO_2}, new measurements from space will help constrain water stress, forest mortality, and plant functional diversity, and aid in understanding mechanisms and differences between the tropical continents. We expect that a synergistic use of multiple satellite observations and a long time series of spatially resolved fluxes derived from sustained satellite observations will enable more process-based understanding and, ultimately, improved carbon-climate model projections.

Materials and methods

We quantify and attribute the NBE to constituent carbon fluxes by assimilating multiple types of satellite observations. The land biosphere net carbon flux NBE $(F_{bio})_i$ at any grid point can be written as

$$(F_{bio})_i = -g_i + s_i + r_i$$

where, g_i, s_i, and r_i are GPP, biomass burning, and total ecosystem respiration at the same grid point. In the above equation, positive means releasing carbon into the atmosphere. The land net biosphere fluxes, GPP (g_i), and biomass-burning (s_i) carbon fluxes were constrained with X_{CO_2} from OCO-2 and GOSAT, SIF from GOSAT (*31*), and CO observations from MOPITT (*34*) separately (fig. S6). Once these quantities are calculated, respiration is calculated as a residual. The error variance of respiration is the sum of GPP, biomass burning, and land biosphere flux error variance.

We use the CMS-Flux (*25*–*27*) inversion framework to estimate monthly mean land and ocean NBE fluxes assuming accurate fossil fuel emissions. The CMS-Flux optimizes surface fluxes with a 4D-Var approach with the GEOS-Chem adjoint model. The GEOS-Chem transport model and its adjoint are run at 4° by 5° resolution driven by GEOS-5 (*64*) (before year 2014) and GEOS-FP meteorology (after year 2014). A Monte Carlo approach is used to estimate the uncertainties of posterior fluxes at each grid. The regional posterior flux uncertainties are the standard deviations of the regionally aggregated ensemble posterior fluxes from the Monte Carlo method. To isolate the impact of prior fluxes on the posterior flux changes between years 2015–2016 and 2011, we use the same prior biosphere fluxes and uncertainties for years 2011 and 2015–2016.

We use a Bayesian analysis framework to estimate monthly average GPP at 4° by 5° grid spacing (consistent with CMS-Flux grid) that optimally accounts for uncertainties in predictions of GPP from terrestrial biosphere models, satellite observations of GOSAT-SIF, and relationships between SIF and GPP (*32*). GOSAT-SIF from Level 2 product was scaled to monthly GPP using the empirical linear relationship with Max Planck Institute (MPI) GPP from 2009–2011 with careful accounting for uncertainties in SIF measurements and the MPI approach (*32*, *33*). MPI GPP is derived from a flux tower data–based upscaling approach using the Max Planck Institute for Biogeochemistry (MPI-BGC) model. The posterior GPP and uncertainties are calculated with least square linear combination of the scaled SIF observations and the prior GPP based on their uncertainties. This approach has been used to examine large-scale GPP distributions and regional GPP responses to climate variability and drought, and has been extensively validated against flux tower data (*33*).

The carbon fluxes from biomass burning are estimated as a multiplication between CO_2:CO emission ratio and the CO carbon fluxes optimized with MOPITT v6 CO observations. The CO emission optimization follows (*35*), which optimize monthly CO emissions independently with initial conditions for each month estimated from a suboptimal Kalman filter (*65*). The CO_2:CO emission ratio ($r_{CO_2:CO}$) at each grid point is calculated using CO_2 and CO emission factors (e_{co_2}, e_{co}) and dry mass matter (m_v) for six vegetation types used in GEOS-Chem

$$r_{CO_2:CO} = \frac{\sum_{i=1}^{6} (e_{CO_2})_i \cdot m_i}{\sum_{i=1}^{6} (e_{CO})_i \cdot m_i}$$

where i represents vegetation types that include agriculture waste, deforestation, extratropical forest, peat, savanna, and woodland. The emission ratio for peat fire over Indonesia is based on field measurement from (*36*). We carried out 6-year inversion from 2010 to 2015. The uncertainty of the posterior biomass fluxes is based on the Monte Carlo method (*25*).

We carried out a series of validation and evaluation to test the robustness of the conclusion, including comparing posterior and prior CO_2 concentration from flux inversion against independent aircraft and surface flask observations (*66*), comparing OCO-2 and GOSAT observations to X_{CO_2} from the TCCON (*30*, *67*–*81*), and estimating the impact of GOSAT and OCO-2 sampling differences on posterior fluxes with OSSEs. The comparison to independent data shows that the OCO-2 and GOSAT X_{CO_2} have consistent error statistics, and the OSSEs indicate that the conclusions from this study are not sensitive to the sampling differences between OCO-2 and GOSAT.

REFERENCES AND NOTES

1. N. Zeng, A. Mariotti, P. Wetzel, Terrestrial mechanisms of interannual CO_2 variability. *Global Biogeochem. Cycles* **19**, GB1016 (2005). doi: 10.1029/2004GB002273
2. P. M. Cox *et al*., Sensitivity of tropical carbon to climate change constrained by carbon dioxide variability. *Nature* **494**, 341–344 (2013). doi: 10.1038/nature11882; pmid: 23389447
3. W. Wang *et al*., Variations in atmospheric CO_2 growth rates coupled with tropical temperature. *Proc. Natl. Acad. Sci. U.S.A.* **110**, 13061–13066 (2013). doi: 10.1073/pnas.1219683110; pmid: 23884654
4. P. M. Cox, R. A. Betts, C. D. Jones, S. A. Spall, I. J. Totterdell, Acceleration of global warming due to carbon-cycle feedbacks in a coupled climate model. *Nature* **408**, 184–187 (2000). doi: 10.1038/35041539; pmid: 11089968
5. P. Friedlingstein *et al*., Climate–carbon cycle feedback analysis: Results from the C^4MIP Model Intercomparison. *J. Clim.* **19**, 3337–3353 (2006). doi: 10.1175/JCLI3800.1
6. I. Y. Fung, S. C. Doney, K. Lindsay, J. John, Evolution of carbon sinks in a changing climate. *Proc. Natl. Acad. Sci. U.S.A.* **102**, 11201–11206 (2005). doi: 10.1073/pnas.0504949102; pmid: 16061800
7. P. Ciais *et al*., Current systematic carbon-cycle observations and the need for implementing a policy-relevant carbon observing system. *Biogeosciences* **11**, 3547–3602 (2014). doi: 10.5194/bg-11-3547-2014
8. D. Schimel *et al*., Observing terrestrial ecosystems and the carbon cycle from space. *Glob. Chang. Biol.* **21**, 1762–1776 (2015). doi: 10.1111/gcb.12822; pmid: 25472464

9. J. B. Fisher *et al*., African tropical rainforest net carbon dioxide fluxes in the twentieth century. *Philos. Trans. R. Soc. Lond. B Biol. Sci.* **368**, 20120376 (2013). doi: 10.1098/rstb.2012.0376; pmid: 23878340
10. D. Schimel, B. B. Stephens, J. B. Fisher, Effect of increasing CO_2 on the terrestrial carbon cycle. *Proc. Natl. Acad. Sci. U.S.A.* **112**, 436–441 (2015). doi: 10.1073/pnas.1407302112; pmid: 25548156
11. W. R. L. Anderegg *et al*., Tropical nighttime warming as a dominant driver of variability in the terrestrial carbon sink. *Proc. Natl. Acad. Sci. U.S.A.* **112**, 15591–15596 (2015). pmid: 26644555
12. D. Crisp, C. E. Miller, P. L. DeCola, NASA Orbiting Carbon Observatory: Measuring the column averaged carbon dioxide mole fraction from space. *J. Appl. Remote Sens.* **2**, 023508 (2008). doi: 10.1117/1.2898457
13. S. D. Polade, D. W. Pierce, D. R. Cayan, A. Gershunov, M. D. Dettinger, The key role of dry days in changing regional climate and precipitation regimes. *Sci. Rep.* **4**, 4364 (2014). doi: 10.1038/srep04364; pmid: 24621567
14. J. D. Neelin, C. Chou, H. Su, Tropical drought regions in global warming and El Niño teleconnections. *Geophys. Res. Lett.* **30**, 2275 (2003). doi: 10.1029/2003GL018625
15. R. Chadwick, P. Good, G. Martin, D. P. Rowell, Large rainfall changes consistently projected over substantial areas of tropical land. *Nat. Clim. Chang.* **6**, 177–181 (2016).
16. Y. Malhi, J. Wright, Spatial patterns and recent trends in the climate of tropical rainforest regions. *Philos. Trans. R. Soc. Lond. B Biol. Sci.* **359**, 311–329 (2004). doi: 10.1098/rstb.2003.1433; pmid: 15212087
17. R. A. Betts, C. D. Jones, J. R. Knight, R. F. Keeling, J. J. Kennedy, El Niño and a record CO_2 rise. *Nat. Clim. Chang.* **6**, 806–810 (2016). doi: 10.1038/nclimate3063
18. T. F. Keenan *et al*., Recent pause in the growth rate of atmospheric CO_2 due to enhanced terrestrial carbon uptake. *Nat. Commun.* **7**, 13428 (2016). doi: 10.1038/ncomms13428; pmid: 27824333
19. C. Le Quéré *et al*., Global carbon budget 2016. *Earth Syst. Sci. Data* **8**, 605–649 (2016). doi: 10.5194/essd-8-605-2016
20. A. Chatterjee *et al*., Influence of El Niño on atmospheric CO_2 over the tropical Pacific Ocean: Findings from NASA's OCO-2 mission. *Science* **358**, eaam5776 (2017).
21. B. Poulter *et al*., Contribution of semi-arid ecosystems to interannual variability of the global carbon cycle. *Nature* **509**, 600–603 (2014). doi: 10.1038/nature13376; pmid: 24847888
22. J. A. Marengo *et al*., The drought of Amazonia in 2005. *J. Clim.* **21**, 495–516 (2008). doi: 10.1175/2007JCLI1600.1; pmid: 18270160
23. J. A. Marengo, J. Tomasella, L. M. Alves, W. R. Soares, D. A. Rodriguez, The drought of 2010 in the context of historical droughts in the Amazon region. *Geophys. Res. Lett.* **38**, L12703 (2011). doi: 10.1029/2011GL047436
24. T. Yokota *et al*., Global concentrations of CO_2 and CH_4 retrieved from GOSAT: First preliminary results. *Sci. Online Lett. Atmos.* **5**, 160–163 (2009). doi: 10.2151/sola.2009-041
25. J. Liu *et al*., Carbon monitoring system flux estimation and attribution: Impact of ACOS-GOSAT X_{CO2} sampling on the inference of terrestrial biospheric sources and sinks. *Tellus B Chem. Phys. Meterol.* **66**, 22486 (2014). doi: 10.3402/tellusb.v66.22486
26. J. Liu, K. W. Bowman, M. Lee, Comparison between the Local Ensemble Transform Kalman Filter (LETKF) and 4D-Var in atmospheric CO_2 flux inversion with the Goddard Earth Observing System-Chem model and the observation impact diagnostics from the LETKF. *J. Geophys. Res. Atmos.* **121**, 13,066–13,087 (2016). doi: 10.1002/2016JD025100
27. K. W. Bowman *et al*., Global and Brazilian carbon response to El Niño Modoki 2011–2010. *Earth Space Sci.* **4**, ea000204 (2017). doi: 10.1002/2016ea000204
28. See supplementary materials.
29. A. Eldering *et al*., The Orbiting Carbon Observatory-2 early science investigations of regional carbon dioxide fluxes, *Science* **358**, eaam5745 (2017).
30. D. Wunch *et al*., The total carbon column observing network. *Philos. Trans. A Math. Phys. Eng. Sci.* **369**, 2087–2112 (2011). doi: 10.1098/rsta.2010.0240; pmid: 21502178
31. C. Frankenberg *et al*., New global observations of the terrestrial carbon cycle from GOSAT: Patterns of plant fluorescence with gross primary productivity. *Geophys. Res. Lett.* **38**, L17706 (2011). doi: 10.1029/2011GL048738
32. N. C. Parazoo *et al*., Terrestrial gross primary production inferred from satellite fluorescence and vegetation models. *Glob. Chang. Biol.* **20**, 3103–3121 (2014). doi: 10.1111/gcb.12652; pmid: 24909755
33. N. Parazoo *et al*., Influence of ENSO and the NAO on terrestrial carbon uptake in the Texas–northern Mexico region. *Global Biogeochem. Cycles* **29**, 1247–1265 (2015). doi: 10.1002/2015GB005125
34. M. N. Deeter *et al*., Vertical resolution and information content of CO profiles retrieved by MOPITT. *Geophys. Res. Lett.* **31**, L15112 (2004). doi: 10.1029/2004GL020235
35. Z. Jiang *et al*., Impact of model errors in convective transport on CO source estimates inferred from MOPITT CO retrievals. *J. Geophys. Res. Atmos.* **118**, 2073–2083 (2013). doi: 10.1002/jgrd.50216
36. C. E. Stockwell *et al*., Field measurements of trace gases and aerosols emitted by peat fires in Central Kalimantan, Indonesia, during the 2015 El Niño. *Atmos. Chem. Phys.* **16**, 11711–11732 (2016). doi: 10.5194/acp-16-11711-2016
37. Y. Yin *et al*., Variability of fire carbon emissions in equatorial Asia and its nonlinear sensitivity to El Niño. *Geophys. Res. Lett.* **43**, 10,472–10,479 (2016). doi: 10.1002/2016GL070971
38. V. Huijnen *et al*., Fire carbon emissions over maritime southeast Asia in 2015 largest since 1997. *Sci. Rep.* **6**, 26886 (2016). doi: 10.1038/srep26886; pmid: 27241616
39. S. E. Page *et al*., The amount of carbon released from peat and forest fires in Indonesia during 1997. *Nature* **420**, 61–65 (2002). doi: 10.1038/nature01131; pmid: 12422213
40. J. C. Jiménez-Muñoz *et al*., Record-breaking warming and extreme drought in the Amazon rainforest during the course of El Niño 2015–2016. *Sci. Rep.* **6**, 33130 (2016). doi: 10.1038/srep33130; pmid: 27604976
41. S. L. Lewis, P. M. Brando, O. L. Phillips, G. M. F. van der Heijden, D. Nepstad, The 2010 Amazon drought. *Science* **331**, 554 (2011). doi: 10.1126/science.1200807; pmid: 21292971
42. C. E. Doughty *et al*., Drought impact on forest carbon dynamics and fluxes in Amazonia. *Nature* **519**, 78–82 (2015). doi: 10.1038/nature14213; pmid: 25739631
43. C. B. Alden *et al*., Regional atmospheric CO_2 inversion reveals seasonal and geographic differences in Amazon net biome exchange. *Glob. Chang. Biol.* **22**, 3427–3443 (2016). doi: 10.1111/gcb.13305; pmid: 27124119
44. L. V. Gatti *et al*., Drought sensitivity of Amazonian carbon balance revealed by atmospheric measurements. *Nature* **506**, 76–80 (2014). doi: 10.1038/nature12957; pmid: 24499918
45. I. T. van der Laan-Luijkx *et al*., Response of the Amazon carbon balance to the 2010 drought derived with CarbonTracker South America. *Global Biogeochem. Cycles* **29**, 1092–1108 (2015). doi: 10.1002/2014GB005082
46. S. L. Lewis, P. M. Brando, O. L. Phillips, G. M. F. van der Heijden, D. Nepstad, The 2010 Amazon drought. *Science* **331**, 554 (2011). doi: 10.1126/science.1200807; pmid: 21292971
47. P. Ciais *et al*., The carbon balance of Africa: Synthesis of recent research studies. *Phil. Trans. R. Soc. A* **369**, 2038–2057 (2011). doi: 10.1098/rsta.2010.0328
48. X. Wang *et al*., A two-fold increase of carbon cycle sensitivity to tropical temperature variations. *Nature* **506**, 212–215 (2014). doi: 10.1038/nature12915; pmid: 24463514
49. Y. Malhi *et al*., Climate change, deforestation, and the fate of the Amazon. *Science* **319**, 169–172 (2008). doi: 10.1126/science.1146961; pmid: 18048654
50. P. B. Duffy, P. Brando, G. P. Asner, C. B. Field, Projections of future meteorological drought and wet periods in the Amazon. *Proc. Natl. Acad. Sci. U.S.A.* **112**, 13172–13177 (2015). doi: 10.1073/pnas.1421010112; pmid: 26460046
51. A. Russo, A. F. Marchese, J. Sillmann, G. Immé, When will unusual heat waves become normal in a warming Africa? *Environ. Res. Lett.* **11**, 054016 (2016). doi: 10.1088/1748-9326/11/5/054016; pmid: 26215178
52. K. Steinkamp, N. Gruber, Decadal trends of ocean and land carbon fluxes from a regional joint ocean-atmosphere inversion. *Global Biogeochem. Cycles* **29**, 2108–2126 (2015). doi: 10.1002/2014GB004907
53. R. J. W. Brienen *et al*., Long-term decline of the Amazon carbon sink. *Nature* **519**, 344–348 (2015). doi: 10.1038/nature14283; pmid: 25788097
54. H. Ivancic, L. P. Koh, Evolution of sustainable palm oil policy in Southeast Asia. *Cogent Environ. Sci.* **2**, 1195032 (2016). doi: 10.1080/23311843.2016.1195032
55. W. R. Anderegg *et al*., Pervasive drought legacies in forest ecosystems and their implications for carbon cycle models. *Science* **349**, 528–532 (2015). doi: 10.1126/science.aab1833; pmid: 26228147
56. P. M. Brando *et al*., Drought effects on litterfall, wood production and belowground carbon cycling in an Amazon forest: Results of a throughfall reduction experiment. *Philos. Trans. R. Soc. Lond. B Biol. Sci.* **363**, 1839–1848 (2008). doi: 10.1098/rstb.2007.0031; pmid: 18267902
57. T. L. Powell *et al*., Confronting model predictions of carbon fluxes with measurements of Amazon forests subjected to experimental drought. *New Phytol.* **200**, 350–365 (2013). doi: 10.1111/nph.12390; pmid: 23844931
58. M. Reichstein *et al*., Climate extremes and the carbon cycle. *Nature* **500**, 287–295 (2013). doi: 10.1038/nature12350; pmid: 23955228
59. J. Zscheischler *et al*., Carbon cycle extremes during the 21st century in CMIP5 models: Future evolution and attribution to climatic drivers. *Geophys. Res. Lett.* **41**, 8853–8861 (2014). doi: 10.1002/2014GL062409
60. D. Frank *et al*., Effects of climate extremes on the terrestrial carbon cycle: Concepts, processes and potential future impacts. *Glob. Chang. Biol.* **21**, 2861–2880 (2015). doi: 10.1111/gcb.12916; pmid: 25752680
61. H. Kreft, W. Jetz, Global patterns and determinants of vascular plant diversity. *Proc. Natl. Acad. Sci. U.S.A.* **104**, 5925–5930 (2007). doi: 10.1073/pnas.0608361104; pmid: 17379667
62. S. L. Lewis *et al*., Above-ground biomass and structure of 260 African tropical forests. *Philos. Trans. R. Soc. Lond. B Biol. Sci.* **368**, 20120295 (2013). doi: 10.1098/rstb.2012.0295; pmid: 23878327
63. I. J. Polonsky, D. M. O'Brien, J. B. Kumer, C. W. O'Dell, Performance of a geostationary mission, geoCARB, to measure CO_2, CH_4 and CO column-averaged concentrations. *Atmos. Meas. Tech.* **7**, 959–981 (2014). doi: 10.5194/amt-7-959-2014
64. M. M. Rienecker *et al*., The GEOS-5 data assimilation system-documentation of versions 5.0.1 and 5.1.0, and 5.2.0 (NASA Tech. Rep. Series on Global Modeling and Data Assimilation, PublicationTM-2008-104606, NASA, 2008), vol. 27.
65. M. Parrington *et al*., Estimating the summertime tropospheric ozone distribution over North America through assimilation of observations from the Tropospheric Emission Spectrometer. *J. Geophys. Res.* **113**, D18307 (2008). doi: 10.1029/2007JD009341
66. K. A. Masarie, W. Peters, A. R. Jacobson, P. P. Tans, ObsPack: A framework for the preparation, delivery, and attribution of atmospheric greenhouse gas measurements. *Earth Syst. Sci. Data* **6**, 375–384 (2014). doi: 10.5194/essd-6-375-2014
67. N. Deutscher *et al*., TCCON data from Bialystok, Poland, Release GGG2014R1, TCCON data archive, hosted by Carbon Dioxide Information Analysis Center (CDIAC) (2014). doi: 10.14291/tccon.ggg2014.bialystok01.R1/1183984
68. J. Notholt *et al*., TCCON data from Bremen, Germany, Release GGG2014R0. TCCON data archive, hosted by Carbon Dioxide Information Analysis Center (CDIAC) (2014). doi: 10.14291/tccon.ggg2014.bremen01.R0/1149275
69. D. W. T. Griffith *et al*., TCCON data from Darwin, Australia, Release GGG2014R0. TCCON data archive, hosted by Carbon Dioxide Information Analysis Center (CDIAC) (2014). doi: 10.14291/tccon.ggg2014.darwin01.R0/1149290
70. K. Strong *et al*., TCCON data from Eureka, Canada, Release GGG2014R0. TCCON data archive, hosted by Carbon Dioxide Information Analysis Center (CDIAC) (2014). doi: 10.14291/tccon.ggg2014.eureka01.R0/1149271
71. R. Sussmann and M. Rettinger, TCCON data from Garmisch, Germany, Release GGG2014R0. TCCON data archive, hosted by Carbon Dioxide Information Analysis Center (CDIAC) (2014). doi: 10.14291/tccon.ggg2014.garmisch01.R0/1149299
72. K. Shiomi *et al*., TCCON data from Saga, Japan, Release GGG2014R0. TCCON data archive, hosted by Carbon Dioxide Information Analysis Center (CDIAC) (2014). doi: 10.14291/tccon.ggg2014.saga01.R0/1149283
73. F. Hase *et al*., TCCON data from Karlsruhe, Germany, Release GGG2014R1. TCCON data archive, hosted by Carbon Dioxide Information Analysis Center (CDIAC) (2014). doi: 10.14291/tccon.ggg2014.karlsruhe01.R1/1182416
74. V. Sherlock *et al*., TCCON data from Lauder, New Zealand, 125HR, Release GGG2014R0. TCCON data archive, hosted by Carbon Dioxide Information Analysis Center (CDIAC), (2014). doi: 10.14291/tccon.ggg2014.lauder02.R0/1149298
75. P. O. Wennberg *et al*., TCCON data from Lamont, Oklahoma, USA, Release GGG2014R1. TCCON data archive, hosted by Carbon Dioxide Information Analysis Center (CDIAC), (2014). doi: 10.14291/tccon.ggg2014.lamont01.R1/1255070

76. T. Warneke *et al.*, TCCON data from Orleans, France, Release GGG2014R0. TCCON data archive, hosted by Carbon Dioxide Information Analysis Center (CDIAC) (2014). doi: 10.14291/tccon.ggg2014.orleans01.R0/1149276
77. P. O. Wennberg *et al.*, TCCON data from Park Falls, Wisconsin, USA, Release GGG2014R0. TCCON data archive, hosted by Carbon Dioxide Information Analysis Center (CDIAC) (2014). doi: 10.14291/tccon.ggg2014.parkfalls01.R0/1149161
78. R. Kivi *et al.*, TCCON data from Sodankyla, Finland, Release GGG2014R0. TCCON data archive, hosted by Carbon Dioxide Information Analysis Center (CDIAC) (2014). doi: 10.14291/tccon.ggg2014.sodankyla01.R0/1149280
79. I. Morino *et al.*, TCCON data from Tsukuba, Ibaraki, Japan, 125HR, Release GGG2014R1. TCCON data archive, hosted by Carbon Dioxide Information Analysis Center (CDIAC) (2014). doi: 10.14291/tccon.ggg2014.tsukuba02.R1/1241486
80. D. W. T. Griffith *et al.*, TCCON data from Wollongong, Australia, Release GGG2014R0. TCCON data archive, hosted by Carbon Dioxide Information Analysis Center (CDIAC) (2014). doi: 10.14291/tccon.ggg2014.wollongong01.R0/1149291
81. D. Wunch *et al.*, Comparisons of the Orbiting Carbon Observatory-2 (OCO-2) X_{CO2} measurements with TCCON. *Atmos. Meas. Tech.* **10**, 2209–2238 (2017). doi: 10.5194/amt-10-2209-2017

ACKNOWLEDGMENTS

This research was carried out at the Jet Propulsion Laboratory, California Institute of Technology, under a contract with the National Aeronautics and Space Administration (NASA). All the computations were performed on the NASA Ames supercomputers. The data used in this study can be obtained from http://cmsflux.jpl.nasa.gov/DS-Science.aspx. This work was supported in part by the NASA Carbon Monitoring System program (grant 14-CMS14-0054) and the NASA Orbiting Carbon Observatory Science team program (grant 14-OCO2_14-0007 and 11-OCO211-0024). K.R.G. acknowledges the NSF Faculty Early Career Developent Program award (CAREER 0846358).

SUPPLEMENTARY MATERIALS

www.sciencemag.org/content/358/6360/eaam5690/suppl/DC1
Materials and Methods
Supplementary Text
Figs. S1 to S13
Table S1
References (*82*–*97*)

9 December 2016; accepted 6 July 2017
10.1126/science.aam5690

Contrasting carbon cycle responses of the tropical continents to the 2015–2016 El Niño

Junjie Liu, Kevin W. Bowman, David S. Schimel, Nicolas C. Parazoo, Zhe Jiang, Meemong Lee, A. Anthony Bloom, Debra Wunch, Christian Frankenberg, Ying Sun, Christopher W. O'Dell, Kevin R. Gurney, Dimitris Menemenlis, Michelle Gierach, David Crisp and Annmarie Eldering

Science **358** (6360), eaam5690.
DOI: 10.1126/science.aam5690